

Article

Synthesis, Optical Characterization in Solution and Solid-State, and DFT Calculations of 3-Acetyl and 3-(1'-(2'-Phenylhydrazono)ethyl)-coumarin-(7)-substituted Derivatives

Cesar A. Villa-Martínez ¹, Nancy E. Magaña-Vergara ^{2,*}, Mario Rodríguez ³, Juan P. Mojica-Sánchez ⁴, Ángel A. Ramos-Organillo ¹, Joaquín Barroso-Flores ^{5,6}, Itzia I. Padilla-Martínez ⁷ and Francisco J. Martínez-Martínez ^{1,*}

- ¹ Facultad de Ciencias Químicas, Universidad de Colima, Km 9 Carretera Coquimatlán-Colima, Coquimatlán 28400, Mexico; cvmartinez@uacol.mx (C.A.V.-M.); aaramos@uacol.mx (Á.A.R.-O.)
 - ² CONACyT, Facultad de Ciencias Químicas, Universidad de Colima, Km 9 Carretera Coquimatlán-Colima, Coquimatlán 28400, Mexico
 - ³ Centro de Investigaciones en Óptica A. P. 1-948, León 37000, Mexico; mrodri@cio.mx
 - ⁴ Tecnológico Nacional de Mexico, Instituto Tecnológico José Mario Molina Pasquel y Henríquez Campus Tamazula de Gordiano, Carretera Tamazula-Santa Rosa No. 329, Tamazula de Gordiano 49650, Mexico; juan.mojica@tamazula.tecmm.edu.mx
 - ⁵ Centro Conjunto de Investigación en Química Sustentable UAEM-UNAM, Unidad San Cayetano, Carretera Toluca-Atlatomulco Km.14.5, Toluca de Lerdo 50200, Mexico; jbarroso@unam.mx
 - ⁶ Instituto de Química, Universidad Nacional Autónoma de Mexico, Circuito Exterior, Ciudad Universitaria, Ciudad de Mexico 04510, Mexico
 - ⁷ Laboratorio de Química Supramolecular y Nanociencias, UPIBI, Instituto Politécnico Nacional, Av. Acueducto s/n Barrio la Laguna Ticomán, Ciudad de Mexico 07340, Mexico; ipadillamar@ipn.mx
- * Correspondence: nancymv@uacol.mx (N.E.M.-V.); fjmartin@uacol.mx (F.J.M.-M.); Tel.: +52-312-3161163 (F.J.M.-M.)



Citation: Villa-Martínez, C.A.; Magaña-Vergara, N.E.; Rodríguez, M.; Mojica-Sánchez, J.P.; Ramos-Organillo, Á.A.; Barroso-Flores, J.; Padilla-Martínez, I.I.; Martínez-Martínez, F.J. Synthesis, Optical Characterization in Solution and Solid-State, and DFT Calculations of 3-Acetyl and 3-(1'-(2'-Phenylhydrazono)ethyl)-coumarin-(7)-substituted Derivatives. *Molecules* **2022**, *27*, 3677. <https://doi.org/10.3390/molecules27123677>

Academic Editor: Petko Petkov

Received: 13 April 2022

Accepted: 2 June 2022

Published: 8 June 2022

Publisher's Note: MDPI stays neutral with regard to jurisdictional claims in published maps and institutional affiliations.



Copyright: © 2022 by the authors. Licensee MDPI, Basel, Switzerland. This article is an open access article distributed under the terms and conditions of the Creative Commons Attribution (CC BY) license (<https://creativecommons.org/licenses/by/4.0/>).

Abstract: Intramolecular charge transfer (ICT) effects are responsible for the photoluminescent properties of coumarins. Hence, optical properties with different applications can be obtained by ICT modulation. Herein, four 3-acetyl-2H-chromen-2-ones (**1a–d**) and their corresponding fluorescent hybrids 3-(phenylhydrazono)-chromen-2-ones (**2a–d**) were synthesized in 74–65% yields. The UV-Vis data were in the 295–428 nm range. The emission depends on the substituent in position C-7 bearing electron-donating groups. Compounds **1b–d** showed good optical properties due to the D- π -A structural arrangement. In compounds **2a–d**, there is a quenching effect of fluorescence in solution. However, in the solid, an increase is shown due to an aggregation-induced emission (AIE) effect given by the rotational restraints and stacking in the crystal. Computational calculations of the HOMO-LUMO orbitals indicate high absorbance and emission values of the molecules, and gap values represent the bathochromic effect and the electronic efficiency of the compounds. Compounds **1a–d** and **2a–d** are good candidates for optical applications, such as OLEDs, organic solar cells, or fluorescence markers.

Keywords: coumarins; hydrazones; optical properties; HOMO-LUMO orbitals

1. Introduction

Intramolecular charge transfer (ICT), as well as linear and nonlinear optical properties [1–5], are associated with organic molecules having an extended electronic π -backbone. This molecular characteristic is generally modulated by the insertion of electron-donor or -acceptor groups into the electronic π -system, to favor the ICT [6]. The typical electronic architectures that can be presented, are donor-acceptor-donor (D-A-D), donor- π -acceptor (D- π -A), or donor- π -acceptor- π -donor (D- π -A- π -D), known as push-pull type compounds.

Photoluminescent compounds and materials with fluorescent and phosphorescent properties play a fundamental role in many areas, such as biology, pharmacology, chemistry, biomedicine, and optoelectronics [7–12]. For example, coumarin compounds coupled to phenylhydrazine have been reported as fluorescent probes for visualizing living tissues [13]. Photoluminescent organic compounds derived from coumarins have been applied in two-photon absorption phenomena, optical data storage, energy limitation, and the manufacture of lasers [5]. Coumarins can be obtained in good yields [9] through synthetic techniques, such as Knoevenagel, Pechmann, and Wittig reactions. Therefore, the photophysical properties of coumarins can be easily modified by substituting in positions 3, 6, 7, and 8 to obtain hybrid materials [9,14,15], which exhibit high quantum yields, important changes in Stokes shifts, and good absorption and emission profiles [16]. On the other hand, fluorescent hybrid compounds derived from hydrazines and coumarins have shown synergic effects in their fluorescent properties [17,18]. These compounds have been applied as on-off sensors [19,20], photoluminescent dyes [21], anticonvulsants [22], hydrogels [23], and antimicrobials [24].

In this work, we describe the synthesis, structural characterization, and photoluminescence properties of small compounds derived from 3-acetyl-2H-chromene-2-one (**1a–d**) coupled with phenylhydrazine, forming the hybrid fluorescent compounds 3-(1'-(2'-phenylhydrazono) ethyl)-2H-2-chromen-2-one (**2a–d**). The optical characterization of **2a–d** was performed in solution and in the solid-state, and the results contrasted with *ab initio* theoretical calculations. The UV-vis spectra of coumarins **1a,c** and **2b** have been reported in solution but not in the solid-state [25,26].

2. Experimental

2.1. Materials and Methods

Salicylaldehyde, 4-methoxy-salicylaldehyde, 4-hydroxy-salicylaldehyde, 4-diethylamino-salicylaldehyde, ethyl acetoacetate, piperidine, glacial acetic acid, ethanol, and phenylhydrazine were purchased from Aldrich (Toluca, Mexico) and used as received. The ACS grade solvents were purchased from CTR (Jalisco, Mexico) and used without further purification. Melting points were measured on an Electrothermal Mel-Temp 1201D apparatus. IR spectra were collected using Varian 3100 FT-IR EXCALIBUR series spectrophotometer. ^1H and ^{13}C NMR spectra were recorded in a BRUKER Ultrashield plus 400 MHz in DMSO- d_6 solutions using $(\text{CH}_3)_4\text{Si}$ as an internal reference compound; chemical shifts (δ) are in ppm and coupling constants ($^nJ_{\text{H-H}}$) in Hz. Mass analysis was performed by electro spray ionization in a high-resolution mass spectrometer Bruker micOTQF- QTOF instrument (Bruker Daltonik GmbH, Bremen, Germany). Absorbances were obtained with a Perkin Elmer Lambda 900 UV/Vis/IR spectrophotometer; emissions were obtained in an Edinburan F55 fluorometer, employing the stock solutions of 1×10^{-3} M of compounds **1a–d** and **2a–d**. The fluorescence spectra were recorded under 400 nm excitation (except in the compound **2d** was in 372 nm). The quantum efficiencies were obtained using an integration sphere of direct photon counting, relating the absorbed and emitted photons. The optical data in the solid state were obtained similarly.

2.2. General Methods of Synthesis and Characterization

3-Acetyl-2H-chromene-2-one (**1a–d**) were prepared following reported procedures [15,27] with modifications. 4-Substituted-salicylaldehydes, ethyl acetoacetate, and piperidine were dissolved in 15 mL of ethanol and placed under reflux at 78 °C for 24 h. After cooling, the solvent was removed by vacuum filtration, and the resulting solid was recrystallized from cold ethanol.

3-Acetyl-2-chromen-2-one (**1a**) [25]. Obtained from salicylaldehyde (0.42 mL, 4.1 mmol), ethyl acetoacetate (0.51 mL, 4.1 mmol), and piperidine (17.4 μL , 3 drops). White solid, yield = 0.62 g (80%), mp = 94–96 °C. λ Abs (nm) = 297 (THF), 296 (acetonitrile). IR (cm^{-1}): ν (C-H) 2978, ν (C-H aromatic) 3047, ν (C=C) 1674–1450, ν (C=O) 1681, ρ (C-H f.p) 771.

¹H-NMR (DMSO-d₆), δ (ppm): 8.67 (1H, s, H-4), 7.95 (1H, d, ³J 8.3, H-5), 7.74 (1H, dd, ³J 7.7, 7.3, H-7), 7.48 (1H, d, ³J 7.7, H-8), 7.44 (1H, d, ³J 8.3, 7.3, H-6), 2.51 (3H, s, H-12). ¹³C-NMR (DMSO-d₆), δ (ppm): 195.5 (C-11), 158.8 (C-2), 155.0 (C-9), 147.4 (C-4), 134.9 (C-7), 131.2 (C-5), 125.4 (C-6), 124.9 (C-3), 118.6 (C-10), 116.5 (C-8), 30.4 (C-12).

3-Acetyl-7-diethylamino-2-chromen-2-one (**1b**) [28,29]. Obtained from 4-diethylamino-salicylaldehyde (0.500 g, 2.6 mmol), ethyl acetoacetate (0.32 mL, 2.6 mmol) and piperidine (17.4 μL, 3 drops). Yellow solid, yield = 0.37 g (59%), mp = 156–158 °C. λ Abs (nm) = 426 (THF), 429 (acetonitrile), 424 (toluene), λ Em (nm) = 466 (THF), 477 (acetonitrile), 461 (toluene). IR (cm⁻¹): ν (C-H) 2924, ν (C-H aromatic) 2962, ν (C=C) 1608–1411, ν (C=O) 1658, ν (C-N) 1188, ρ (C-H f.p) 759. ¹H-NMR (DMSO-d₆), δ (ppm): 8.4 (1H, s, H-4), 7.65 (1H, d, ³J 9.0, H-5), 6.78 (1H, dd, ³J 9.0, ⁴J 2.4, H-6), 6.56 (1H, d, ⁴J 2.3, H-8), 3.9 (3H, s, H-12), 3.49 (4H, q, ³J 7.0, N (CH₂CH₃)₂), 1.14 (6H, t, ³J 7.0, N (CH₂CH₃)₂). ¹³C-NMR (DMSO-d₆), δ (ppm): 194.6 (C-11), 160.3 (C-2), 158.7 (C-9), 153.4 (C-7), 148.0 (C-4), 132.8 (C-5), 115.5 (C-3), 110.6 (C-6), 107.9 (C-10), 96.3 (C-8), 44.8 (N (CH₂CH₃)₂), 12.8 (N (CH₂CH₃)₂).

3-Acetyl-7-hydroxy-2-chromen-2-one (**1c**) [30]. Obtained from 4-hydroxy-salicylaldehyde (0.500 g, 3.62 mmol), ethyl acetoacetate (0.42 mL, 3.6 mmol) and piperidine (17.4 μL, 3 drops). Green solid, yield = 0.68 g (89%), mp = 240–242 °C. λ Abs (nm) = 359 (THF), 356 (acetonitrile), λ Em (nm) = 460 (THF), 453 (acetonitrile). IR (cm⁻¹): ν (C-H) 2927; ν (C-H aromatic) 3032, ν (C=C) 1678–1450, ν (C=O) 1678; ν (O-H) 3194, ρ (C-H f.p) 763. ¹H-NMR (DMSO-d₆), δ (ppm): 8.57 (1H, s, H-4), 7.65 (1H, d, ³J 8.6, H-5), 6.86 (1H, dd, ³J 8.6, ⁴J 2.2, H-6), 6.73 (1H, d, ⁴J 2.2, H-8), 2.63 (3H, s, H-12). ¹³C-NMR (DMSO-d₆), δ (ppm): 195.1 (C-11), 165.1 (C-2), 159.5 (C-9), 157.8 (C-7), 148.2 (C-4), 133.1 (C-5), 119.4 (C-3), 114.8 (C-6), 111.1 (C-10), 102.2 (C-8), 30.4 (C-12).

3-Acetyl-7-methoxy-2-chromen-2-one (**1d**) [31]. Obtained from 4-methoxy-salicylaldehyde (0.500 g, 3.28 mmol), ethyl acetoacetate (0.41 mL, 3.3 mmol) and piperidine (17.4 μL, 3 drops). Yellow solid, yield = 0.63 g (87%), mp = 172–174 °C. λ Abs (nm) = 356 (THF), 354 (acetonitrile). IR (cm⁻¹): ν (C-H) 2978, ν (C-H aromatic) 3032, ν (C=C) 1666–1462, ν (C=O) 1670, ν (C-O-C) 1126, ρ (C-H f.p) 767. ¹H-NMR (DMSO-d₆), δ (ppm): 8.62 (1H, s, H-4); 7.86 (1H, d, ³J 8.6, H-5), 7.02 (1H, dd, ³J 8.6, H-6), 7.04 (1H, s, H-8), 2.56 (3H, s, H-12), 3.9 (3H, s, OMe). ¹³C-NMR (DMSO-d₆), δ (ppm): 195.1 (C-11), 165.3 (C-2), 159.3 (C-9), 157.5 (C-7), 148.0 (C-4), 132.6 (C-5), 120.8 (C-3), 113.9 (C-6), 112.2 (C-10), 100.7 (C-8), 56.7 (OMe), 30.4 (C-12).

Compounds **2a,c** were prepared according to previous reports [31]. Compounds **2b,d** have not been reported yet. The corresponding 4-substituted compound **1a–d**, phenylhydrazine, and glacial acetic acid were added to 10 mL of ethanol and refluxed at 78 °C for 4 h. The solvent was removed by gravity filtration, and the solid was washed with ethanol, recrystallized from ethanol at room temperature, and then characterized.

3-(1-(2-Phenylhydrazono) ethyl) 2-chromen-2-one (**2a**) [32]. Obtained from **1a** (0.300 g, 1.07 mmol), phenylhydrazine (0.105 mL, 1.07 mmol) and glacial acetic acid (13.6 μL, 3 drops). Orange solid, yield = 0.39 g (74%), mp = 184–186 °C. λ Abs (nm) = 277 (THF), 275 (acetonitrile). IR (cm⁻¹): ν (C-H) 2978, ν (C-H aromatic) 3032, ν (C=C) 1597–1489, ν (NH) 3294, ν C=N (1597), ρ (C-H f.p) 732. ¹H-NMR (DMSO-d₆), δ (ppm): 9.46 (NH, s), 8.20 (1H, s, H-4), 7.84 (1H, d, ³J 7.8, H-5), 7.60 (1H, dd, ³J 7.9, 7.4, H-7), 7.41 (1H, d, ³J 8.0, H-8), 7.36 (1H, dd, ³J 7.9, 7.5, H-6), 7.21–7.27 (4H, *o, m, -Ph*), 6.79 (1H, *p, -Ph*), 2.23 (3H, s, H-12), ¹³C-NMR (DMSO-d₆), δ (ppm): 160.4 (C-2), 153.4 (C-9), 146.0 (C-11), 139.6 (C-4), 139.1 (*ipso, -Ph*), 132.0 (C-7), 129.3 (C-5), 129.2 (*m, -Ph*), 127.8 (C-3), 125.0 (C-6), 119.8 (C-10), 119.7 (*p, -Ph*), 116.3 (C-8), 113.5 (*o, -Ph*), 15.5 (C-12).

7-(Diethylamino)-3-(1-(2-phenylhydrazono)ethyl)2-chromen-2-one (**2b**). Obtained from **1b** (0.300 g, 1.15 mmol), phenylhydrazine (0.113 mL, 1.15 mmol) and glacial acetic acid (13.6 μL,

3 drops). Orange solid, yield = 0.32 g (65%), mp = 236–238 °C. λ Abs (nm) = 411 (THF), 413 (acetonitrile), 408 (toluene), λ Em (nm) = 479 (THF), 494 (acetonitrile), 469 (toluene). IR (cm⁻¹): ν (C-H) 2900; ν (C-H aromatic) 2966; ν (C=C) 1589–1408, ν (NH) 3302, ν C=N (1589), ρ (C-H f.p) 748. ¹H-NMR (DMSO-d₆), δ (ppm): 9.23 (NH, s), 8.01 (1H, s, H-4), 7.56 (1H, d, ³J 8.9, H-5), 7.22–7.20 (4H, *o, m*, -Ph), 6.73 (1H, *p*, -Ph), 6.71 (1H, d, ³J 8.9, H-6), 6.55 (1H, s, H-8), 2.20 (3H, s, H-12), 3.45 (4H, *q*, ³J 6.9, N (CH₂CH₃)₂), 1.14 (6H, *t*, ³J 7.0, N (CH₂CH₃)₂), ¹³C-NMR (DMSO-d₆), δ (ppm): 160.9 (C-2), 156.4 (C-9), 150.9 (C-7), 146.4 (C-11), 140.4 (*ipso*, -Ph), 140.6 (C-4), 130.2 (C-5), 129.2 (*m*, -Ph), 120.1 (C-3), 119.3 (*p*, -Ph), 113.4 (*m*, -Ph), 109.7 (C-6), 108.6 (C-10), 96.6 (C-8), 44.5 (N (CH₂CH₃)₂), 15.7 (C-12), 12.8 (N (CH₂CH₃)₂). MS-MS (ESI) m/z = 350.1866 [M + H]⁺ (experimental), 350.1869 (calculated).

7-(Hydroxy)-3-(1-(2-phenylhydrazono)ethyl)-2-chromen-2-one (**2c**) [26]. Obtained from **1c** (0.300 g, 1.46 mmol), phenylhydrazine (0.144 mL, 1.46 mmol) and glacial acetic acid (13.6 μ L, 3 drops). Yellow solid, yield = 0.36 g (65%), mp = 228–230 °C. λ Abs (nm) = 278 (THF), 276 (acetonitrile), λ Em (nm) = 465 (THF). IR (cm⁻¹): ν (C-H aromatic) 3032; ν (C=C) 1593–1442, ν (NH) 3325, ν (O-H) 3221 ν (C=N) 1597, ρ (C-H f.p) 748. ¹H-NMR (DMSO-d₆), δ (ppm): 10.62 (1H, s, OH) 9.31 (NH, s), 8.09 (1H, s, H-4), 7.66 (1H, d, ³J 8.4, H-5), 6.81 (1H, d, ³J 8.4, H-6), 6.74 (1H, s, H-8), 7.22 (4H, *o, p*, -Ph), 6.77 (1H, *p*, -Ph), 2.20 (3H, s, H-12). ¹³C-NMR (DMSO-d₆), δ (ppm): 161.6 (C-7), 160.4 (C-2), 155.5 (C-9), 146.0 (C-11), 140.4 (C-4), 139.7 (*ipso*, -Ph), 130.6 (C-5), 129.2 (*m*, -Ph), 123.3 (C-3), 119.6 (*p*, -Ph), 113.9 (C-6), 113.4 (*o*, -Ph), 112.2 (C-10), 102.2 (C-8), 15.6 (C-12).

7-(Methoxy)-3-(1-(2-phenylhydrazono)ethyl)-2-chromen-2-one (**2d**). Obtained from **1d** (0.300 g, 1.48 mmol), phenylhydrazine (0.148 mL, 1.46 mmol) and glacial acetic acid (13.6 μ L, 3 drops). Yellow solid, yield = 0.41 g (65%), mp = 228–230 °C. λ Abs (nm) = 278 (THF), 275 (acetonitrile), λ Em (nm) = 467 (THF). IR (cm⁻¹): ν (C-H) 2997, ν (C-H aromatic) 3020, ν (C=C) 1612–1496, ν (NH) 3309, ν (C=N) 1608, ρ (C-H f.p) 736. ¹H-NMR (DMSO-d₆), δ (ppm): 9.36 (NH, s), 8.15 (1H, s, H-4), 7.77 (1H, d, ³J 8.65 H-5), 7.23–7.22 (4H, *o, m*, -Ph); 7.0 (1H, s, H-8), 6.98 (1H, d, ³J 8.6, H-6), 6.79 (1H, *p*, -Ph), 3.88 (3H, s, OMe), 2.21 (3H, s, H-12), ¹³C-NMR (DMSO-d₆), δ (ppm): 162.8 (C-2), 160.3 (C-2), 155.4 (C-9), 146.1 (C-11), 140.1 (C-4), 139.5 (*ipso*, -Ph), 130.3 (C-5), 129.3 (*m*, -Ph), 124.3 (C-3), 119.6 (*p*, -Ph), 113.5 (C-6), 113.3 (*o*, -Ph), 113.3 (C-6), 100.7 (C-8), 56.4 (OMe), 15.5 (C-12). MS-MS (ESI) m/z = 309.1235 [M + H]⁺ (experimental), 309.1239 (calculated).

2.3. Determination of Quantum Yield

Fluorescence quantum yield (Φ) for coumarins (**1a–d**) and hydrazones (**2a–d**) were measured through the integration sphere direct excitation method, with “Direct Excitation” measurements, which record the scatter and the emission of the sample being directly excited by the radiation from the excitation monochromator only. The absolute fluorescence quantum yield (Φ) is the ratio of the number of photons emitted to the number of photons absorbed, according to Equation (1).

$$\phi = \frac{N^{em}}{N^{abs}} \quad (1)$$

The absolute fluorescence quantum yield (Φ_{Dexc}) was calculated with the direct excitation method according to Equation (2).

$$\phi_{Dexc} = \frac{E_B - E_A}{S_A - S_B} \quad (2)$$

where E denotes the emission region of sample and solvent, S the excitation scatter region of sample and solvent, and A, B the experimental setup and integral of the scans of samples and solvent.

For calculating the integrals, the selection of the integral regions, and the final calculation of Φ_{Dexc} , we used the quantum yield wizard supplied with the equipment software [33].

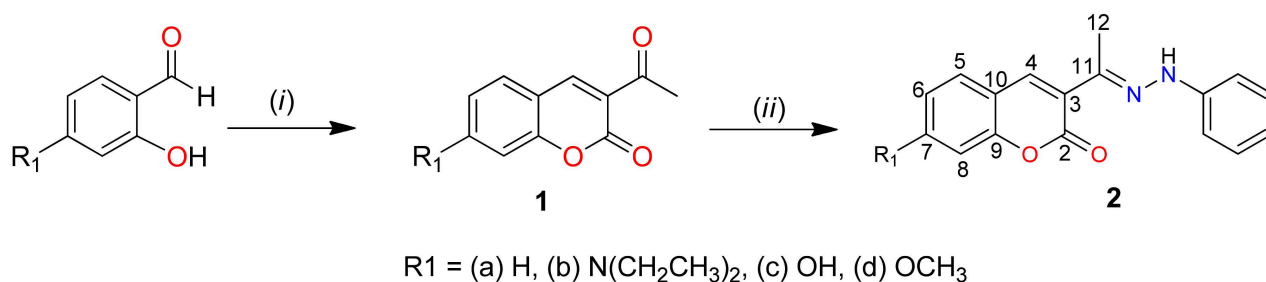
2.4. Computational Details

Geometry optimizations were carried out using the framework of density functional theory implemented in ORCA software [34]. For the exchange and correlation, the PBE0 hybrid functional [35,36] was combined with a complete electronic basis set aug-cc-pVDZ [37]. A vibrational frequency analysis was effectuated to verify minima energy states; only positive values were found in all cases. The HOMO-LUMO gap energies were calculated, and frontier orbitals were plotted using Chemcraft [38]. Excited states were determined using TD-DFT [39–41] under the same level of theory PBE0/aug-cc-pVDZ [42], and solvent effects were included using a conductor-like polarizable model (CPCM) [43,44] considering THF, acetonitrile, and toluene.

3. Results and Discussion

3.1. Synthesis and Structural Characterization

Coumarins **1a–d** were synthesized by the Knoevenagel [28] condensation of ethyl acetoacetate with the corresponding 4-substituted salicylaldehyde (Scheme 1), with yields higher than 80%. Afterward, the functionalization of 3-acetyl-coumarin derivatives **1a–d** with phenylhydrazine was performed through acid catalysis with glacial acetic acid to obtain compounds **2a–d** (Scheme 1). The experimental yields are in the 65–74% range, according to precise reports about the synthesis of the same compounds [2,29,32,45].



(i) Piperidine, EtOH, reflux 24 h; (ii) AcOH(cat), EtOH, reflux 24 h

Scheme 1. Synthesis of 3-acetyl-2H-chromen-2-one (**1a–d**) and 3-(1-(2-phenylhydrazone)ethyl)-2-chromen-2-one (**2a–d**).

The H-4 signal in the ¹H NMR spectra indicated the formation of compounds **1a–d** (Figures S1–S8), appearing in the 8.40–8.67 ppm range [31]. The functionalization with phenylhydrazine in compounds **2a–d**, generated an anisotropic effect perpendicularly extended from the phenyl group of the hydrazone fragment to the pyran ring, causing the protection of H-4 and shifting the signal to lower frequencies in the 8.00–8.15 ppm range. The NH proton in the phenylhydrazone was shifted to high frequencies appearing in the 9.31–9.46 ppm range; whereas the ¹³C-NMR signal was shielded from 194.6–195.5 ppm, for compounds **1a–d**, to the range of 146.0–146.4 ppm in compounds **2a–d** (Figures S9–S16). The IR spectra of compounds **1a–d** showed the C=O band in the 1658–1681 cm⁻¹ range. Meanwhile, compounds **2a–d** showed the characteristic hydrazone C=N and N-H bands in the 1589–1608 cm⁻¹ and 3294–3325 cm⁻¹ ranges, respectively. Selected ¹H and ¹³C NMR values and IR wavenumbers are listed in Table 1.

Table 1. Selected ^1H , ^{13}C NMR ($\delta = \text{ppm}$, DMSO- d_6) and IR ($\nu = \text{cm}^{-1}$) spectroscopic data for compounds **1a–d** and **2a–d**.

Comp.	δ ^1H	δ ^{13}C	ν/cm^{-1}	Comp.	δ ^1H	δ ^{13}C	ν/cm^{-1}	ν/cm^{-1}
	H-4	C-11	C=O		H-4	N-H	C=N	N-H
								C=N
1a	8.67	195.5	1681	2a	8.00	9.46	146.0	3294
1b	8.40	194.6	1658	2b	8.01	9.23	146.4	3302
1c	8.57	195.1	1678	2c	8.09	9.31	146.0	3325
1d	8.62	195.1	1670	2d	8.15	9.36	146.1	3309

3.2. UV-vis Absorption and Photoluminescence Spectra

The UV-vis and fluorescence spectroscopic data of compounds **1a–d** and **2a–d**, measured in tetrahydrofuran and acetonitrile solvents at room temperature, are listed in Table 2. Their scarce solubility in solvents, such as ethanol, DMF, and water, limited the tests in these solvents. The absorption and emission spectra in solution are shown in Figures 1 and 2, respectively. The maximum absorbance bands are attributed to $\pi \rightarrow \pi^*$ and $n \rightarrow \pi^*$ electronic transitions. The absorption band in **1b–d** showed a red-shift due to the insertion of electron-donor substituents in the C-7 position. The largest red-shift in **1b** is attributed to the strong electron-donor character of the diethylamino group [4,9]. Similar behavior is conserved in phenylhydrazone derivatives, wherein **2b** shows the largest bathochromic effect in the absorption band. The molar absorptivity depends on the solvent used, obtaining higher values with acetonitrile than with THF. In contrast to the full palette observed in the absorption, compounds **1a,d** and **2a** showed no emission band. The maximum wavelength of the coumarin emission band is around 453–494 nm. The increase of emission is related to the nature of the substituent in C-7 following the order: $\text{N}(\text{CH}_2\text{CH}_3)_2 > \text{OH} > \text{OCH}_3 > \text{H}$, in agreement with the strength of the substituent electron-donor properties [4,9]. Compound **1b** showed the largest quantum yield (Φ_F) with values above 80%.

Table 2. Experimental photophysical properties in a solution of compounds **1a–d** and **2a–d**.

Compound	Solvent	λ_{maxAbs}	ϵ ($\text{M}^{-1} \text{cm}^{-1}$)	λ_{maxEm}	Stokes Shift (cm^{-1})	Φ_F (%)
1a	THF	297	100,870	NO	NO	NO
	Acetonitrile	296	138,563	NO	NO	NO
1b	THF	426	42,277	466	2014	6
	Acetonitrile	429	45,357	477	2345	80
1c	THF	359	194,444	460	6116	>1
	Acetonitrile	356	196,477	453	6014	>1
1d	THF	356	238,403	NO	NO	NO
	Acetonitrile	354	244,724	NO	NO	NO
2a	THF	277	21,480	NO	NO	NO
	Acetonitrile	275	268,504	NO	NO	NO
2b	THF	411	31,247	479	3454	>1
	Acetonitrile	413	39,880	494	3970	2
2c	THF	278	16,525	465	14465	>1
	Acetonitrile	276	235,090	NO	NO	NO
2d	THF	278	17,588	467	14557	>1
	Acetonitrile	275	237,623	NO	NO	NO

THF = Tetrahydrofuran, Quantum Yield (Φ_F). $\lambda^{\text{ex}}(\text{Em}) = \lambda_{\text{max}}(\text{Abs})$. NO Not Observed.

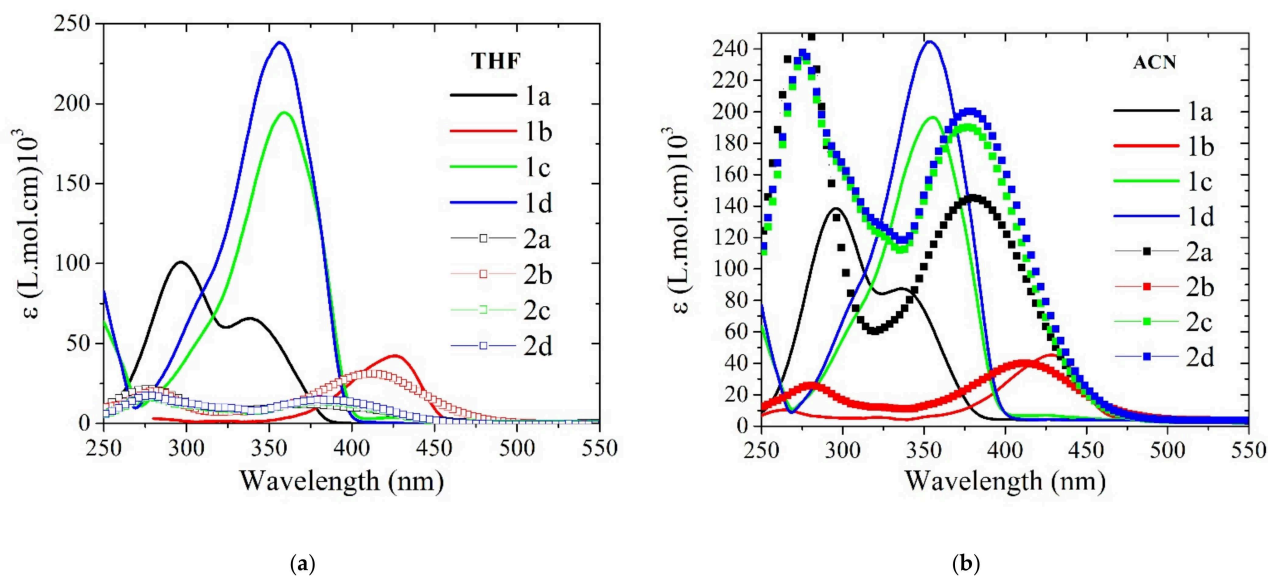


Figure 1. Absorption UV-vis spectra of compounds **1a–d** and **2a–d** ($c = 1 \times 10^{-4}$ M, at 25 °C) in (a) THF, and (b) acetonitrile.

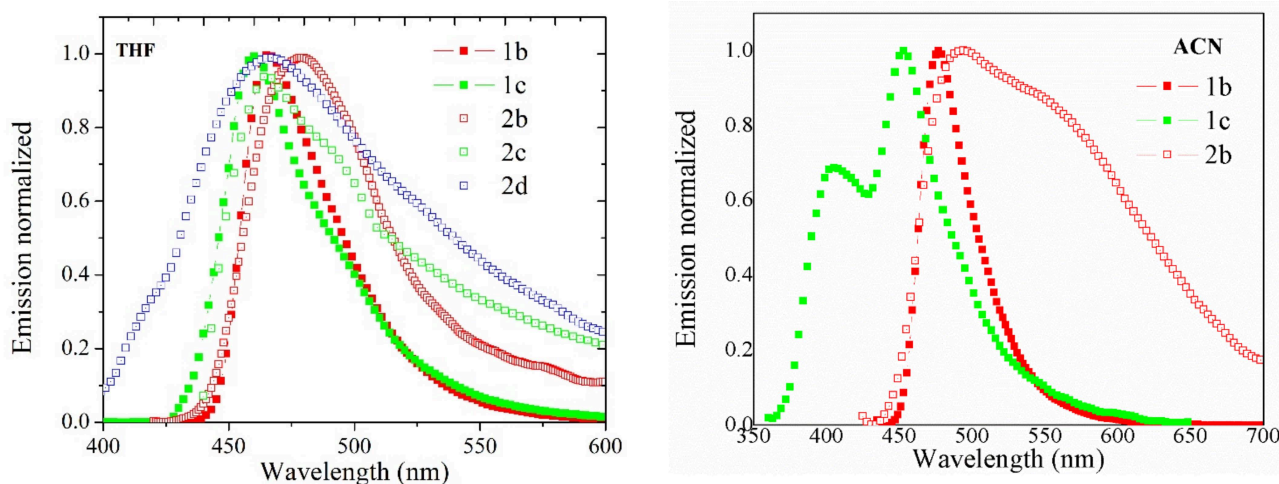


Figure 2. Fluorescence spectra of compounds **1b,c**, **2b–d** in THF and **1b,c**, **2b** in acetonitrile solutions ($c = 1 \times 10^{-4}$ M, at 25 °C). λ^{ex} (Em) = λ_{max} (Abs). Compound **2c,d** do not have emission.

On the other hand, a brief comparison between the photophysical properties of coumarins **1a–d** with the corresponding values of hydrazones **2a–d** allowed us to conclude that coumarin functionalization in the C-3 position with hydrazine caused fluorescence quenching with null fluorescence yields. This result is explained by the diminished electron acceptor capabilities of the resulting hydrazone functionality.

Compounds **1b,d**, and **2c** showed the best photophysical properties in the solid-state. Their fluorescence spectra are shown in Figure 3, and their photophysical properties are listed in Table 3. The emission λ_{max} of coumarin **1b** was red-shifted to 595 nm in comparison with the solution (477 nm), and unexpectedly, compound **1d** turned emissive, showing a band at 540 nm, although with low Φ_{F} values (<6.6%) in both cases. In contrast, hydrazone **2c** has emissive properties compared to the solution: emission at 582 nm and Φ_{F} value of 52.6. These results revealed that the intermolecular interactions in the solid-state favor the emissive relaxation mechanism from an excited state. The X-ray molecular structures of compounds **1a,b,d** are known [46–49]. Hence, a brief analysis of their photoluminescent properties in relation with their molecular structure in the solid state seems appropriate.

The powder X-ray diffractogram of **1a,b,d** was obtained and compared to the single crystal reported ones, shown in Figure S17. In the solid, the free rotation of the pendant $-OMe$ and $3-Ac$ groups is restricted due to intermolecular hydrogen bonds, leading to a coplanar system and increasing the emissive properties of **1d**. Therefore, the solid-state exerts an aggregation-induced emission (AIE) effect [46] on **1d**. In the solid, the molecules of **1d** are π -stacked along the (100) direction, at a distance of 3.509 \AA between the benzo fused (Bz) and lactone (L) rings centroids (Cg (Bz)-Cg (L)) [47], in agreement with medium strength π -D- π -A interactions arranged in the head-to-tail fashion [50]. It is worth mentioning that the Bz ring acts as the donor and the L ring as the acceptor. In contrast, coumarin **1a** crystallizes in two forms, triclinic (form A) and monoclinic (form B). Form A (herein obtained) is a head-to-head stacked, while form B generates head-to-tail π -stacked dimers with long Cg (Bz)-Cg (L) distances of 4.77 \AA and 3.98 \AA , respectively [48]. On the contrary, an aggregation-caused quenching (ACQ) effect is observed on **1b**. In the crystal lattice, the molecules of **1b** are arranged in dimers through antiparallel type carbonyl-carbonyl interactions [51] at Cg (Bz)-Cg (L) distance of 6.38 \AA and the amino-ethyl groups pointing to opposite directions [49]. The free rotation of the pendant $-NEt_2$ and $3-Ac$ groups in **1b** is restricted as in **1d**, but with the contrary effect. This brief analysis supports that the Φ_F in the solid-state depends on the crystal lattice arrangement. Coumarin molecules that show head-to-tail π -stating arrangement with a Cg(Bz)-Cg(L) distance shorter than 3.5 \AA seem to favor large Φ_F values. The large value of Φ_F of hydrazone **2c** in the solid-state is also explained as an AIE effect. Intermolecular hydrogen bonding, probably between the $-OH$ and the $C=N$ functionality, should favor an entire head-to-tail π -stating arrangement in the crystal lattice with the appropriate Cg (Bz)-Cg (L) distance, as mentioned earlier.

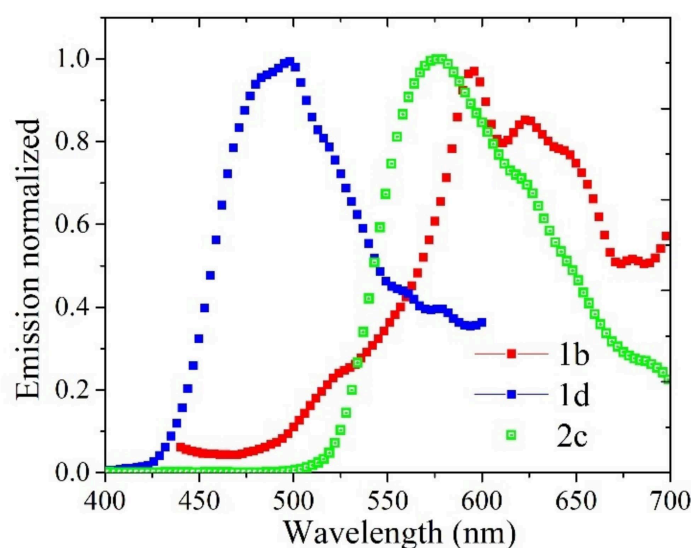


Figure 3. Fluorescence spectra in the solid-state of compounds **1b,d**, and **2c** (at $25 \text{ }^\circ\text{C}$).

Table 3. Photophysical properties of compounds **1b,d**, and **2c** in the solid-state.

Compound	λ_{\max} Em (nm)	Φ_F (%)
1b	595	<1
1d	540	6.6
2c	582	52.6

Compounds **1–5** have been used as fluorescent dyes for cellular imaging (1), indicators of bathochromic effects with red emissions (2), chemosensors for anions (3), for the study of nonlinear optical properties (4), and observation of highly fluorescent compounds depending on the substituents (5). Their photophysical properties are listed in Table 4.

7-Diethylamino substituted coumarin **1b** showed better photophysical properties (Φ_F) in solution than compounds **1–5**, previously reported and shown in Figure 4 [6,7,10,16,52]. Then, compound **1b** in solution and **2c** in the solid-state could be evaluated in similar applications, since they have even better optical properties, and their synthesis is simpler and with higher chemical yields than the reported compounds **1–7**.

Table 4. Reported photophysical properties of 7-diethylamino-coumarins, used for comparison purposes.

Structure	Absorbance (nm)	Emission (nm)	Φ_F (%)	References
1	379	501 (479)	71 (42)	[7]
2	510	585	>1	[16]
3	406	482	>1	[52]
4	432	490	NR	[6]
5	436	544	>1	[10]
6	316	458	NR	[53]
7	527	551	NR	[54]

NR = Not reported; (Emission in solid-state).

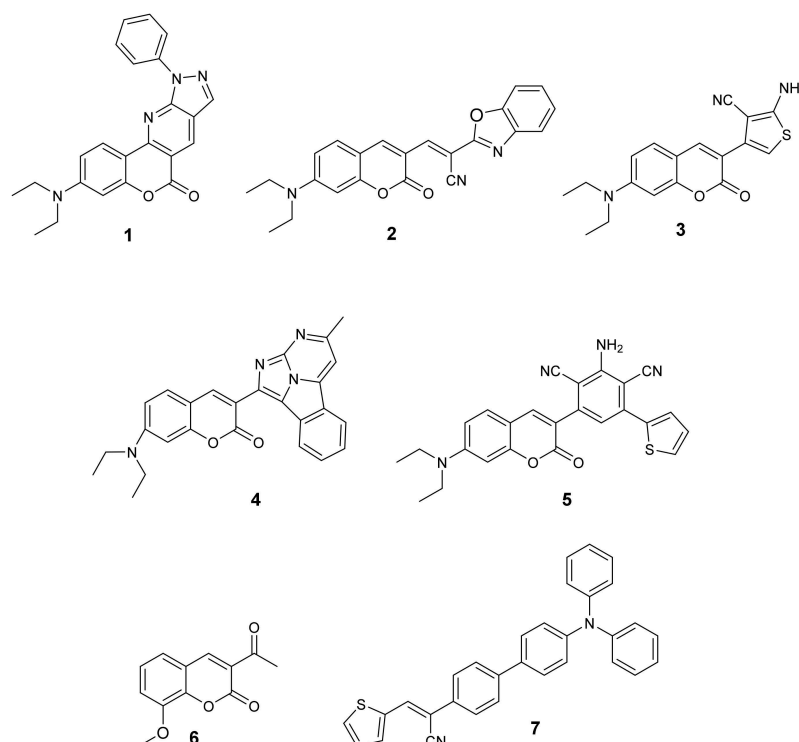


Figure 4. Reported coumarin compounds with photophysical properties in solution, used for comparison purposes [6,7,10,16,52–54].

3.3. Theoretical Calculations

The theoretical data of the molecular orbitals allowed us to explain the spectroscopic behavior and the electronic effects in the molecules. The HOMO (H), LUMO (L), H-L gap, and E_g^{OP} energy values are listed in Table 5. The H-L gap energies are similar among them. Nevertheless, the smallest value corresponds to compound **1b**, whose λ_{max} is displaced towards the red. Likewise, the H-L gap represents the excited state electronic transition [6,38] from S_0 to S_1 . Compounds **2a–d** show low H-L gap values similar to coumarins **1a–d**. The theoretical values, listed in Table 5, agree with the experimental optical values.

Table 5. HOMO-LUMO (H-L) gap values of compounds **1a–d** and **2a–d**. Data are calculated at aug-cc-pVDZ/PBE0 level of theory. Experimental E_{g}^{OP} values are also shown.

Compound	HOMO (eV)	LUMO (eV)	H-L Gap (eV)	E_{g}^{OP} (eV) *
1a	−7.28	−2.80	4.47	4.18
1b	−6.29	−2.44	3.84	2.90
1c	−6.93	−2.60	4.32	3.50
1d	−6.81	−2.53	4.28	3.56
2a	−5.34	−2.51	2.83	4.52
2b	−4.93	−2.05	2.88	3.03
2c	−5.57	−2.57	3.00	3.28
2d	−5.18	−2.29	2.88	3.34

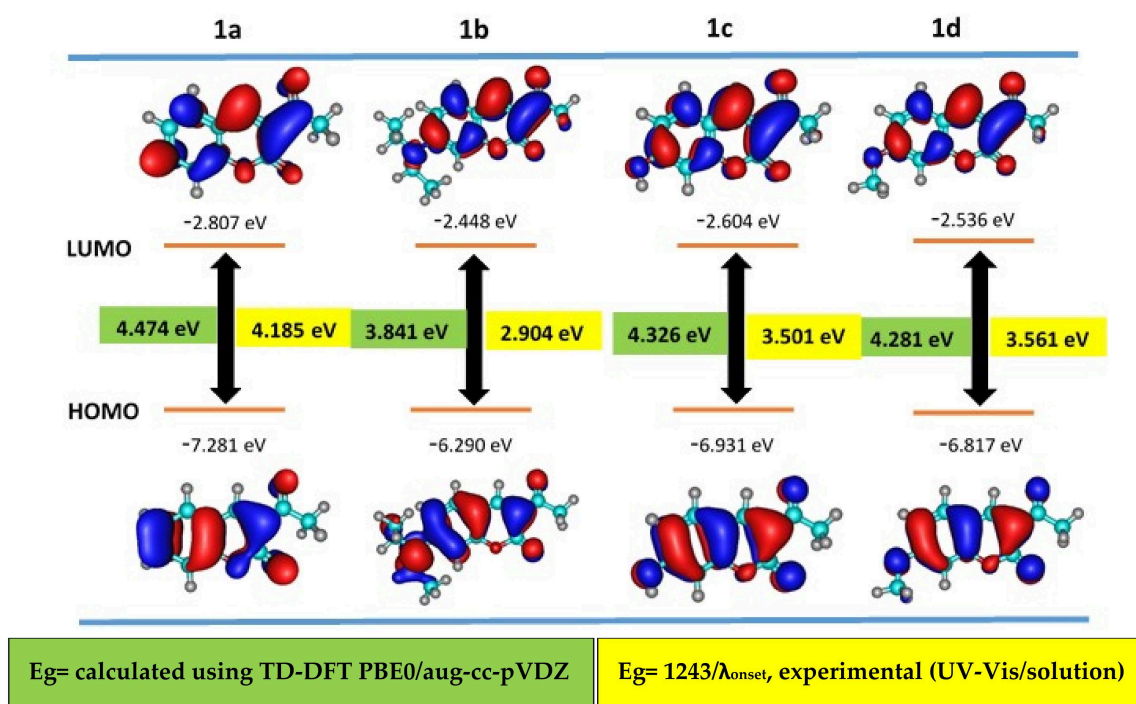
* Obtained from equation $E_{g}^{OP} = 1243/\lambda$ (values obtained from highest wavelengths in Table 2).

The optical gap values (E_{g}^{OP}) for coumarins rank from 2.90 to 4.18 eV, and they are smaller than the theoretical data (3.84–4.47 eV); where compound **1b** shows the smallest E_{g}^{OP} value, indicating good ICT capability. E_{g}^{OP} values of compounds **2a–d** show low energy values (3.03–4.52 eV) like coumarins. These results indicate that the absorbance and emission red-shifts are due to the good electronic efficiency in their D-A structure. The theoretical and experimental H-L gap values are in agreement with the experimental optical properties and increase their possibility to function as semiconductor compounds [55]. The theoretical and experimental H-L gap values are in agreement with the experimental optical properties and increase their possibility to function as semiconductor compounds [55]. The experimental values are comparable with the data for well-known luminophores **3**, **6**, and **7** listed in Table 6 and whose structures are shown in Figure 5.

Table 6. Comparison of reported theoretical calculations with compounds **1a–d** y **2a–d**.

Compounds	HOMO (eV)	LUMO (eV)	Gap (eV)	References
3	−5.68 to −1.83	−2.15 to 0.38	NR	[52]
6	−6.21 to −6.35	−2.39 to −2.51	3.69 to 3.95	[53]
7	−5.17 to −5.34	−2.10 to −3.19	1.98 to 2.47	[54]

NR = Not reported.

**Figure 5.** Frontier molecular orbitals corresponding to the optimized structures of compounds **1a–d**.

The data of compounds **1b–d** showed HOMO-LUMO interactions (Table S1) in a higher percentage of contribution energy due to the ED groups generating $n \rightarrow \pi^*$ transitions, in contrast to compound **1a**, which causes HOMO-1-LUMO $\pi \rightarrow \pi^*$ transitions, in agreement with the experimental data.

Compounds **2a–d** showed $\pi \rightarrow \pi^*$ and $n \rightarrow \pi^*$ transitions represented by the HOMO-LUMO, HOMO+1-LUMO-1 orbitals (supplementary material Table S2), indicating a D-A behavior of the molecules which is consistent with the experimental data.

Figure 5 shows the FMOs (frontier molecular orbitals) of compounds **1a–d**. The structures show a planar geometry through the benzopyran ring. The HOMO-LUMO and HOMO-1-LUMO electronic distributions indicate the presence of $\pi \rightarrow \pi^*$ and $n \rightarrow \pi^*$ transitions, confirming the excitation of the FMOs from S_0 to S_1 .

In compounds **2a–d**, the phenylhydrazine group acts as an ED group. In this case, it represents the energy of the HOMO, and often, the whole part of the coumarin where the substituent in the benzopyrone ring acts as EA group, represented by the energy of the LUMO (Figure 6). The previous result agrees with the experimental findings, suggesting that the electronic cloud of the ED moiety moves towards the EA, which is from the phenylhydrazine to the coumarin. The hydrazone-coumarins **2a–d** showed low quantum yields and unobservable emissions because the electronic cloud does not include the ED group which is interacting with the solvents.

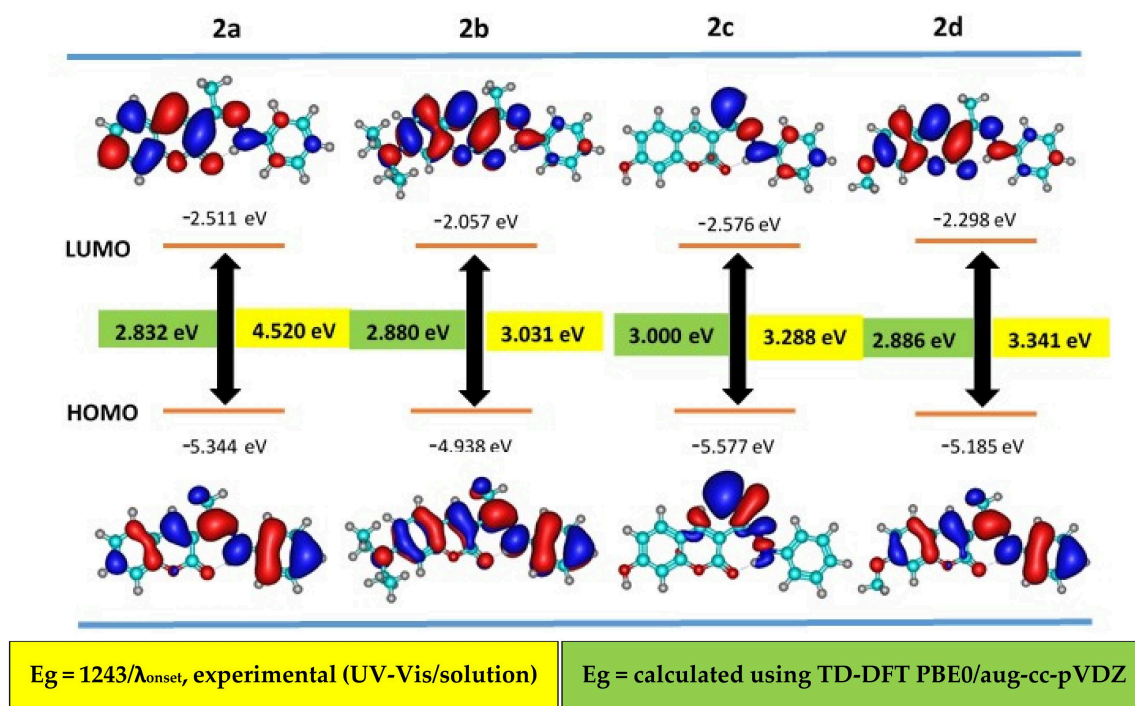


Figure 6. Frontier molecular orbitals corresponding to the optimized structures of compounds **2a–d**.

Compound **2c** shows different behavior in the FMOs, and its electron density is both as HOMO and LUMO in the hydrazone group, generating only $n \rightarrow \pi^*$ type transitions, which agrees with its behavior in the solid-state, since the solvent generates the quenching of the fluorescence in solution.

4. Conclusions

Molecules **1a–d** and **2a–d** can be good candidates for semiconductor compounds suitable to be used in several optical applications. The photophysical properties of coumarins **1a–d** and their hydrazone derivatives **2a–d** were compared. The bandgap indicates the efficient ICT, which confirms the D-A type structure. Compounds **1b** and **2c** presented the best optical properties. Compound **1b** showed absorbances at $\lambda > 420$ nm and emission

at $\lambda > 460$ nm in solution and quantum yields $>80\%$. Compound **2c** also showed good emission values in the solid-state due to the push-pull system, supported by the π - π interactions. Compound **1d** turned emissive in the solid-state due to the π - π interactions in the crystal network. This work also confirms that small coumarins derivatives possess photoluminescent properties which can be tuned in both solution and in the solid-state.

Supplementary Materials: The following supporting information can be downloaded at: <https://www.mdpi.com/article/10.3390/molecules27123677/s1>, Figures S1–S16, ^1H and ^{13}C NMR spectra; Figure S17, Powder X-ray diffractogram of **1a,b,d**; Table S1, HOMO-LUMO interactions of compounds **1b–d**, Table S2, HOMO-LUMO interactions of compounds **2b–d**.

Author Contributions: Conceptualization, F.J.M.-M., M.R. and N.E.M.-V.; Methodology, C.A.V.-M.; Software, J.P.M.-S. and J.B.-F.; Investigation, I.I.P.-M. and Á.A.R.-O.; Writing, C.A.V.-M., F.J.M.-M. and I.I.P.-M. All authors have read and agreed to the published version of the manuscript.

Funding: Partially supported by Universidad de Colima and Consejo Nacional de Ciencia y Tecnología (CONACYT, grants, 316892 and 255354) and SIP-IPN.

Institutional Review Board Statement: Not applicable.

Informed Consent Statement: Not applicable.

Acknowledgments: Centro de Investigaciones en Óptica de León Gto. Mexico. The computational calculations were supported by the high-performance computing system of PIDi-UTEM (SCC-PIDI-UTEM-CONICYT-FONDEQUIP-EQM180180).

Conflicts of Interest: The authors declare no conflict of interest.

Sample Availability: Samples of the compounds **1a–d** and **2a–d** are available from the authors.

References

- Rodríguez-Romero, J.; Aparicio-Ixta, L.; Rodríguez, M.; Ramos-Ortíz, G.; Maldonado, J.L.; Jiménez-Sánchez, A.; Farfán, N.; Santillan, R. Synthesis, chemical-optical characterization and solvent interaction effect of novel fluorene-chromophores with D-A-D structure. *Dyes Pigments* **2013**, *98*, 31–41. [[CrossRef](#)]
- Kamath, P.R.; Sunil, D.; Ajees, A.A.; Pai, K.S.R.; Das, S. Some new indole-coumarin hybrids; synthesis, anticancer and Bcl-2 docking studies. *Bioorg. Chem.* **2015**, *63*, 101–109. [[CrossRef](#)]
- Srinivasa, H.T.; Palakshamurthy, B.S.; Abdulkarim, T.M. Ethyl 7-hydroxycoumarin-3-carboxylate derivatives: Synthesis, characterization and effect of liquid crystal properties. *J. Mol. Struct.* **2018**, *1155*, 513–519. [[CrossRef](#)]
- Akchurin, I.O.; Yakhutina, A.I.; Bochkov, A.Y.; Solovjova, N.P.; Medvedev, M.G.; Traven, V.F. Novel push-pull fluorescent dyes-7-(diethylamino)furo-and thieno [3,2-c] derivatives: Structure, electronic spectra and TD-DFT study. *J. Mol. Struct.* **2018**, *1160*, 216–221. [[CrossRef](#)]
- Zhang, Y.; Shi, Z.; Li, Y. Photoexcitation mechanism of new D- π -A coumarin derivatives in linear and nonlinear optical processes. *J. Mater. Sci.* **2016**, *27*, 7132–7140. [[CrossRef](#)]
- García, S.; Vázquez, J.L.; Rentería, M.; Aguilar, G.I.G.; Delgado, F.; Trejo, D.M.; Garcia, R.M.A.; Alvarado, M.E.; Vazquez, M.A. Synthesis and experimental computational characterization of nonlinear optical properties of triazacyclopentafluorene-coumarin derivatives. *Opt. Mater.* **2016**, *62*, 231–239. [[CrossRef](#)]
- Chen, J.; Liu, W.; Ma, J.; Xu, H.; Tang, X.; Fan, Z.; Wang, P. Synthesis and properties of fluorescence dyes: Tetracyclic pyrazolo [3,4-b]pyridine-based coumarin chromophores with intramolecular charge transfer character. *J. Org. Chem.* **2012**, *77*, 3475–3482. [[CrossRef](#)]
- Bassolino, G.; Nancoz, C.; Thiel, Z.; Bois, E.; Vauthey, E.; Rivera, F.P. Photolabile coumarins with improved efficiency through azetidiny substitution. *Chem. Sci.* **2018**, *9*, 387–391. [[CrossRef](#)] [[PubMed](#)]
- Aksungur, T.; Aydiner, B.; Seferolu, N.; Ozkutuk, M.; Arslan, L.; Reis, Y.; Acik, L.; Seferoglu, Z. Coumarin-indole conjugate donor-acceptor system: Synthesis photophysical properties, anion sensing ability, theoretical and biological activity studies of two coumarin-indole based push-pull dyes. *J. Mol. Struct.* **2017**, *1147*, 364–379. [[CrossRef](#)]
- Aydiner, B.; Yalcin, E.; Korkmaz, V.; Seferoglu, Z. Efficient one-pot three-component method for the synthesis of highly fluorescent coumarin-containing 3,5-disubstituted-2,6-dicyanoaniline derivatives under microwave irradiation. *Synth. Commun.* **2017**, *47*, 2174–2188. [[CrossRef](#)]
- Sinha, S.; Gaur, P.; Dev, S.; Mukhopadhyay, S.; Mukherjee, T.; Ghosh, S. Hydrazine response molecular material: Optical signaling and mushroom cell staining. *Sens Actuators B Chem.* **2015**, *221*, 418–426. [[CrossRef](#)]
- Huang, Y.; Zhang, Y.; Yuan, Y.; Wenwen, C. Organogelators based on iodo 1,2,3-triazole functionalized with coumarin: Properties and gelator solvent interaction. *Tetrahedron.* **2015**, *71*, 2124–2133. [[CrossRef](#)]

13. Li, T.; Wang, L.; Lin, S.; Xu, X.; Liu, M.; Shen, S.; Yan, Z.; Mo, R. Rational design and bioimaging applications of highly specific “Turn-On” fluorescent probe for hypochlorite. *Bioconjugate Chem.* **2018**, *29*, 2838–2845. [CrossRef] [PubMed]
14. Minoru, Y.; Yuma, H.; Hideki, O.; Fumito, T. Photochemical synthesis and photophysical properties of coumarins bearing extended polyaromatic rings studied by emission and transient absorption measurements. *Photochem. Photobiol. Sci.* **2017**, *16*, 555–563. [CrossRef]
15. Arcos, R.R.; Maldonado, D.M.; Ordóñez, H.J.; Romero, A.M.; Farfán, N.; del Pilar Carreón-Castro, M. 3-Substituted-7-(diethylamino)coumarins as molecular scaffolds for the bottom-up self-assembly of solids with extensive π -stacking. *J. Mol. Struct.* **2017**, *1130*, 914–921. [CrossRef]
16. Tathe, A.B.; Gupta, V.D.; Sekar, N. Synthesis and combined experimental and computational investigations on spectroscopic and photophysical properties of red emitting 3-styryl coumarins. *Dyes Pigments* **2015**, *119*, 49–55. [CrossRef]
17. Liangliang, L.; Yanjun, W.; Lin, W.; Aihua, G.; Feilong, H.; Chi, Z. A fluorescent probe for hypochlorite based on the modulation of the unique rotation of the N-N single bond in acetohydrazine. *Chem. Commun.* **2015**, *51*, 10435–10438. [CrossRef]
18. Wu, Q.; Ma, L.; Xu, Y.; Cao, D.; Guan, R.; Liu, Z.; Yu, X. Two Coumarin formhydrazide compounds as chemosensors for copper ions. *Inorg. Chem. Commun.* **2016**, *69*, 7–9. [CrossRef]
19. Essaidi, Z.; Krupka, O.; Iliopoulos, K.; Champigny, E.; Sahraoui, B.; Sallé, M.; Gindre, D. Synthesis and functionalization of coumarin containing copolymers for second order optical nonlinearities. *Opt. Mater.* **2013**, *35*, 576–581. [CrossRef]
20. Mukherjee, K.; Chio, T.I.; Gu, H.; Banerjee, A.; Sorrentino, A.M.; Sackett, D.L.; Bane, S.L. Benzocoumarin hydrazine: A large stoke shift fluorogenic sensor for detecting carbonyls in isolated biomolecules and in live cells. *ACS Sens.* **2017**, *2*, 128–134. [CrossRef] [PubMed]
21. Dai, X.; Zhao, Y.W.; Zhi, F.D.; Jun, Y.M.; Bao, X. Z A simple but effective near infrared ratiometric fluorescent probe for hydrazine and its application in bioimaging. *Sens. Actuator B-Chem.* **2016**, *232*, 369–374. [CrossRef]
22. Dehestani, L.; Ahangar, N.; Hashemi, S.M.; Irannejad, H.; Masihi, P.H.; Shakiba, A.; Emami, S. Design, synthesis, in vivo and in silico evaluation of phenacyl triazole hidrazones as new anticonvulsant agents. *Bioorg. Chem.* **2018**, *78*, 119–129. [CrossRef]
23. Iturmendi, A.; Theis, S.; Maderegger, D.; Monkowius, U.; Teasdale, I. Coumarin caged polyphosphazenes with a visible light driven on demand degradation. *Macromol. Rapid Commun.* **2018**, *39*, 1800377–1800383. [CrossRef] [PubMed]
24. Soni, J.N.; Soman, S.S. Reactions of coumarin-3-carboxylate, its crystallographic study and antimicrobial activity. *Pharma Chem.* **2014**, *6*, 396–403.
25. Ming, K.L.; Jing, L.; Ying, Z.; Xiao, Y.X.; Xin, S.; Zhe, Y.T.; Zheng, H.; Xiao, X.L. Synthesis, photoluminescent behaviors, and antibacterial activities of 3-acetylcoumarins. *Res. Chem. Intermed.* **2015**, *41*, 3289–3296. [CrossRef]
26. Liu, M.; Xu, Z.; Song, Y.; Li, H.; Xian, C. A novel Coumarin Based chemosensor for colorimetric detection of Ag(I) ion and fluorogenic sensing of Ce(III) ion. *J. Lumines.* **2018**, *17*, 31882–311991. [CrossRef]
27. Chimenti, F.; Secci, D.; Bolasco, A.; Chimenti, P.; Granese, A.; Befani, O.; Turini, P.; Alcaro, S.; Ortuso, F. Inhibition of monoamine oxidases by coumarin-3-acyl derivatives: Biological activity and computational study. *Bioorg. Med. Chem. Lett.* **2004**, *14*, 3697–3703. [CrossRef] [PubMed]
28. Valizadeh, H.; Shockravi, A.; Gholipur, H. Microwave assisted synthesis of coumarins via potassium carbonate catalyzed Knoevenagel condensation in 1-*n*-butyl-3-methylimidazolium bromide ionic liquid. *J. Heterocycl. Chem.* **2007**, *44*, 867–871. [CrossRef]
29. Grover, J.; Kumar, V.; Sobhia, M.E.; Jachak, S.M. Synthesis, biological evaluation and docking analysis of 3-methyl-1-phenylchromeno [4,3-*c*]pyrazol-4(1H)-ones as potential cyclooxygenase-2 (COX-2) inhibitors. *Bioorg. Med. Chem. Lett.* **2014**, *24*, 4638–4642. [CrossRef]
30. Dai, X.; Qing, H.W.; Peng, C.W.; Jie, T.; Yu, X.; Sheng, Q.W.; Jun, Y.M.; Bao, X.Z. A simple and effective coumarin based fluorescent probe for cysteine. *Biosens. Bioelectron.* **2014**, *59*, 35–39. [CrossRef] [PubMed]
31. Kumar, J.A.; Saidachary, G.; Mallesham, G.; Sridhar, B.; Jain, N.; Kalivendi, S.V.; Jayathirtha, R.J.; Raju, C.B. Synthesis, anticancer activity and photophysical properties of novel substituted 2-oxo-2H-cromenylpyrazolecarboxylates. *Eur. J. Med. Chem.* **2013**, *65*, 389–402. [CrossRef]
32. Padilla-Martinez, I.; Flores, L.I.Y.; García, B.E.V.; Gonzalez, J.; Cruz, A.; Martinez-Martinez, F.J. X-Ray supramolecular structure, NMR spectroscopy and synthesis of 3-methyl-1-phenyl-1H-cromeno [3,4-*c*]pyrazol-4-ones formed by the unexpected cyclization of 3-[1-(phenyl-hydrazono)ethyl]-cromen-2-ones. *Molecules* **2011**, *16*, 915–932. [CrossRef]
33. *Reference Guide Edinburgh Instruments FLS980*; Integrating sphere for measurements of fluorescence quantum yields and spectral reflectance; Edinburgh Instruments Ltd.: Livingston, UK, 2016.
34. Neese, F. The ORCA program system. *Wiley Interdisciplinary Reviews: Comput. Mol. Sci.* **2012**, *2*, 73–78. [CrossRef]
35. Perdew, J.P.; Ernzerhof, M.; Burke, K. Rationale for mixing exact exchange with density functional approximations. *J. Chem. Phys.* **1996**, *105*, 9982–9985. [CrossRef]
36. Adamo, C.; Barone, V. Toward reliable density functional methods without adjustable parameters: The PBE0 model. *J. Chem. Phys.* **1999**, *110*, 6158–6170. [CrossRef]
37. Kendall, R.A.; Dunning, T.H., Jr.; Harrison, R.J. Electron affinities of the first-row atoms revisited. Systematic basis sets and wave functions. *J. Chem. Phys.* **1992**, *96*, 6796–6806. [CrossRef]
38. Zhurko, G.A. Chemcraft-Graphical Program for Visualization of Quantum Chemistry Computations. Available online: <https://chemcraftprog.com> (accessed on 12 April 2022).

39. Laurent, A.D.; Jacquemin, D. TD-DFT benchmarks: A review. *Int. J. Quantum. Chem.* **2013**, *113*, 2019–2039. [[CrossRef](#)]
40. Jacquemin, D.; Wathelet, V.; Perpète, E.A.; Adamo, C. Extensive TD-DFT benchmark: Singlet-excited states of organic molecules. *J. Chem. Theory Comput.* **2009**, *5*, 2420–2435. [[CrossRef](#)]
41. Charaf-Eddin, A.; Planchat, A.; Mennucci, B.; Adamo, C.; Jacquemin, D. Choosing a functional for computing absorption and fluorescence band shapes with TD-DFT. *J. Chem. Theory Comput.* **2013**, *9*, 2749–2760. [[CrossRef](#)] [[PubMed](#)]
42. Taouali, W.; Casida, M.E.; Znaidia, S.; Alimi, K. Rational design of (DA) copolymers towards high efficiency organic solar cells: DFT and TD-DFT study. *J. Mol. Graph.* **2019**, *89*, 139–146. [[CrossRef](#)] [[PubMed](#)]
43. Takano, Y.; Houk, K.N. Benchmarking the conductor-like polarizable continuum model (CPCM) for aqueous solvation free energies of neutral and ionic organic molecules. *J. Chem. Theory Comput.* **2005**, *1*, 70–77. [[CrossRef](#)]
44. Raj, R.K.; Gunasekaran, S.; Gnanasambandan, T. Combined spectroscopic and DFT studies on 6-bromo-4-chloro-3-formyl coumarin. *Spectrochim. Acta Part A: Mol. Biomol. Spectrosc.* **2015**, *139*, 505–514. [[CrossRef](#)]
45. Grover, J.; Roy, K.S.; Jachak, S.M. Potassium carbonate mediated efficient and convenient synthesis of 3-methyl-1-phenylchromeno [4,3-c]pyrazol-4(1H)-ones. *Synth. Commun.* **2014**, *44*, 1914–1923. [[CrossRef](#)]
46. Luo, J.; Xie, Z.; Lam, J.W.Y.; Cheng, L.; Chen, H.; Qiu, C.; Kwok, H.S.; Zhan, X.; Liu, Y.; Zhu, D.; et al. Aggregation-induced emission of 1-methyl-1,2,3,4,5-pentaphenylsilole. *Chem. Commun.* **2001**, *18*, 1740–1741. [[CrossRef](#)] [[PubMed](#)]
47. Han, H.-M.; Lu, C.-R.; Zhang, Y.; Zhang, D.-C. 3-Acetyl-7-methoxycoumarin. *Acta Crystallogr. Sect. E* **2005**, *61*, o1864. [[CrossRef](#)]
48. Parthapratim, M.; Tayur, N.; Guru, R. Topological Analysis of Charge Density Distribution in Concomitant Polymorphs of 3-Acetylcoumarin, A Case of Packing Polymorphism. *Cryst. Growth Des.* **2006**, *6*, 708–718.
49. Christopher, G.; Hamaker, C.S. McCully, 3-Acetyl-7-(diethyl amino)coumarin. *Acta Crystallogr. Sect. E* **2006**, *62*, o2072–o2074. [[CrossRef](#)]
50. García-Báez, E.V.; Martínez-Martínez, F.J.; Höpfl, H.; Padilla-Martínez, I.I. π -Stacking Interactions and CH \cdot X (X = O, aryl) Hydrogen Bonding as Directing Features of the Supramolecular Self-Association in 3-Carboxy and 3-Amido Coumarin Derivatives. *Cryst. Growth Des.* **2003**, *3*, 35–45. [[CrossRef](#)]
51. Cabrera-Pérez, L.C.; García-Báez, E.V.; Franco-Hernández, M.O.; Martínez-Martínez, F.J.; Padilla-Martínez, I.I. Carbonyl–carbonyl interactions and amide π -stacking as the directing motifs of the supramolecular assembly of ethyl N-(2-acetylphenyl)-oxalamate in a synperiplanar conformation. *Acta Crystallogr. Sect. C* **2015**, *C71*, 381–385. [[CrossRef](#)]
52. Yanar, U.; Babur, B.; Pekyilmaz, D.; Yahaya, I.; Aydiner, B.; Dede, Y.; Seferoglu, Z. A fluorescent coumarin thiophene hybrid as a ratiometric chemosensor for anions: Synthesis, photophysics, anions sensing and orbital interactions. *J. Mol. Struct.* **2016**, *1108*, 269–277. [[CrossRef](#)]
53. Shu, X.; Li, J.; Li, M.-K. Crystal structure photoluminescent and theoretical studies of 3-acetyl-8-methoxy-coumarine derivatives. *Asian J. Chem.* **2014**, *26*, 8427–8430. [[CrossRef](#)]
54. Garcias-Morales, C.; Romero-Borja, D.; Maldonado, J.-L.; Roa, A.E.; Rodríguez, M.; García-Merinos, J.P.; Ariza-Castolo, A. Small Molecules derived from Thieno [3,4-c] pyrrole-4,6-dione (TPD) and their use in solution processed organic solar cells. *Molecules* **2017**, *22*, 1607–1622. [[CrossRef](#)] [[PubMed](#)]
55. Costa, J.C.S.; Taveira, R.J.S.; Lima, C.F.R.A.C.; Mendes, A.; Santos, L.M.N.B.F. Optical band gaps of organic semiconductor materials. *Opt. Mater.* **2016**, *58*, 51–60. [[CrossRef](#)]